DESY 00-037 ISSN 0418-9833
March 2000

Elastic Photoproduction of J/ψ and Υ Mesons at HERA

H1 Collaboration

Abstract

Cross sections for elastic photoproduction of J/ψ and Υ mesons are presented. For J/ψ mesons the dependence on the photon-proton centre-of-mass energy $W_{\gamma p}$ is analysed in an extended range with respect to previous measurements of $26 \leq W_{\gamma p} \leq 285$ GeV. The measured energy dependence is parameterized as $\sigma_{\gamma p} \propto W_{\gamma p}^{\delta}$ with $\delta = 0.83 \pm 0.07$. The differential cross section $d\sigma/dt$ for J/ψ mesons is derived, its dependence on $W_{\gamma p}$ and on t is analysed and the effective trajectory (in terms of Regge theory) is determined to be $\alpha(t) = (1.27 \pm 0.05) + (0.08 \pm 0.17) \cdot t/\mathrm{GeV}^2$. Models based on perturbative QCD and on pomeron exchange are compared to the data.

Submitted to Phys. Lett. B

C. Adloff[33], V. Andreev[24], B. Andrieu[27], V. Arkadov[35], A. Astvatsatourov[35], I. Ayyaz[28], A. Babaev[23], J. Bähr[35], P. Baranov[24], E. Barrelet[28], W. Bartel[10], U. Bassler[28], P. Bate[21], A. Beglarian[34], O. Behnke[10], C. Beier[14], A. Belousov[24], T. Benisch[10], Ch. Berger[1], G. Bernardi[28], T. Berndt[14], J.C. Bizot[26], K. Borras[7], V. Boudry[27], W. Braunschweig[1], V. Brisson[26], H.-B. Bröker[2], D.P. Brown[21], W. Brückner[12], P. Bruel[27], D. Bruncko[16], J. Bürger[10], F.W. Büsser[11], A. Bunyatyan[12,34], H. Burkhardt[14], A. Burrage[18], G. Buschhorn[25], A.J. Campbell[10], J. Cao[26], T. Carli[25], S. Caron[1], E. Chabert[22], D. Clarke[5], B. Clerbaux[4], C. Collard[4], J.G. Contreras[7,41], J.A. Coughlan[5], M.-C. Cousinou[22], B.E. Cox[21], G. Cozzika[9], J. Cvach[29], J.B. Dainton[18], W.D. Dau[15], K. Daum[33,39], M. David[9,†], M. Davidsson[20], B. Delcourt[26], N. Delerue[22], R. Demirchyan[34], A. De Roeck[10,43], E.A. De Wolf[4], C. Diaconu[22], P. Dixon[19], V. Dodonov[12], J.D. Dowell[3], A. Droutskoi[23], C. Duprel[2], G. Eckerlin[10], D. Eckstein[35], V. Efremenko[23], S. Egli[32], R. Eichler[36], F. Eisele[13], E. Eisenhandler[19], M. Ellerbrock[13], E. Elsen[10], M. Erdmann[10,40,e], W. Erdmann[36], P.J.W. Faulkner[3], L. Favart[4], A. Fedotov[23], R. Felst[10], J. Ferencei[10], S. Ferron[27], M. Fleischer[10], G. Flügge[2], A. Fomenko[24], I. Foresti[37], J. Formánek[30], J.M. Foster[21], G. Franke[10], E. Gabathuler[18], K. Gabathuler[32], J. Garvey[3], J. Gassner[32], J. Gayler[10], R. Gerhards[10], S. Ghazaryan[34], L. Goerlich[6], N. Gogitidze[24], M. Goldberg[28], C. Goodwin[3], C. Grab[36], H. Grässler[2], T. Greenshaw[18], G. Grindhammer[25], T. Hadig[1], D. Haidt[10], L. Hajduk[6], T. Hauschildt[11], W.J. Haynes[5], B. Heinemann[18], G. Heinzelmann[11], R.C.W. Henderson[17], S. Hengstmann[37], H. Henschel[35], R. Heremans[4], G. Herrera[7,41], I. Herynek[29], M. Hilgers[36], K.H. Hiller[35], C.D. Hilton[21], J. Hladký[29], P. Höting[2], D. Hoffmann[10], W. Hoprich[12], R. Horisberger[32], S. Hurling[10], M. Ibbotson[21], Ç. İşsever[7], M. Jacquet[26], M. Jaffre[26], L. Janauschek[25], D.M. Jansen[12], X. Janssen[4], V. Jemanov[11], L. Jönsson[20], D.P. Johnson[4], M.A.S. Jones[18], H. Jung[20], H.K. Kästli[36], D. Kant[19], M. Kapichine[8], M. Karlsson[20], O. Karschnick[11], O. Kaufmann[13], M. Kausch[10], F. Keil[14], N. Keller[37], J. Kennedy[18], I.R. Kenyon[3], S. Kermiche[22], C. Kiesling[25], M. Klein[35], C. Kleinwort[10], G. Knies[10], B. Koblitz[25], H. Kolanoski[38], S.D. Kolya[21], V. Korbel[10], P. Kostka[35], S.K. Kotelnikov[24], M.W. Krasny[28], H. Krehbiel[10], J. Kroseberg[37], D. Krücker[38], K. Krüger[10], A. Küpper[33], T. Kuhr[11], T. Kurča[35,16], R. Kutuev[12], W. Lachnit[10], R. Lahmann[10], D. Lamb[3], M.P.J. Landon[19], W. Lange[35], T. Laštovička[30], A. Lebedev[24], B. Leißner[1], R. Lemrani[10], V. Lendermann[7], S. Levonian[10], M. Lindstroem[20], B. List[36], E. Lobodzinska[10,6], B. Lobodzinski[6,10], N. Loktionova[24], V. Lubimov[23], S. Lüders[36], D. Lüke[7,10], L. Lytkin[12], N. Magnussen[33], H. Mahlke-Krüger[10], N. Malden[21], E. Malinovski[24], I. Malinovski[24], R. Maraček[25], P. Marage[4], J. Marks[13], R. Marshall[21], H.-U. Martyn[1], J. Martyniak[6], S.J. Maxfield[18], A. Mehta[18], K. Meier[14], P. Merkel[10], F. Metlica[12], A. Meyer[10], H. Meyer[33], J. Meyer[10], P.-O. Meyer[2], S. Mikocki[6], D. Milstead[18], T. Mkrtchyan[34], R. Mohr[25], S. Mohrdieck[11], M.N. Mondragon[7], F. Moreau[27], A. Morozov[8], J.V. Morris[5], D. Müller[37], K. Müller[13], P. Murín[16,42], V. Nagovizin[23], B. Naroska[11], J. Naumann[7], Th. Naumann[35], I. Négri[22], G. Nellen[25], P.R. Newman[3], T.C. Nicholls[5], F. Niebergall[11], C. Niebuhr[10], O. Nix[14], G. Nowak[6], T. Nunnemann[12], J.E. Olsson[10], D. Ozerov[23], V. Panassik[8], C. Pascaud[26], G.D. Patel[18], E. Perez[9], J.P. Phillips[18], D. Pitzl[10], R. Pöschl[7], I. Potachnikova[12], B. Povh[12], K. Rabbertz[1], G. Rädel[9], J. Rauschenberger[11], P. Reimer[29], B. Reisert[25], D. Reyna[10], S. Riess[11], E. Rizvi[3], P. Robmann[37], R. Roosen[4], A. Rostovtsev[23], C. Royon[9], S. Rusakov[24], K. Rybicki[6], D.P.C. Sankey[5], J. Scheins[1], F.-P. Schilling[13], S. Schleif[14], P. Schleper[13], D. Schmidt[33], D. Schmidt[10], L. Schoeffel[9], A. Schöning[36], T. Schörner[25], V. Schröder[10], H.-C. Schultz-Coulon[10], K. Sedlák[29], F. Sefkow[37], V. Shekelyan[25], I. Sheviakov[24], L.N. Shtarkov[24], G. Siegmon[15], P. Sievers[13], Y. Sirois[27], T. Sloan[17], P. Smirnov[24], V. Solochenko[23], Y. Soloviev[24], V. Spaskov[8], A. Specka[27], H. Spitzer[11], R. Stamen[7], J. Steinhart[11], B. Stella[31], A. Stellberger[14], J. Stiewe[14], U. Straumann[37], W. Struczinski[2], M. Swart[14], M. Taševský[29], V. Tchernyshov[23], S. Tchetchelnitski[23], G. Thompson[19], P.D. Thompson[3], N. Tobien[10], D. Traynor[19], P. Truöl[37], G. Tsipolitis[36], J. Turnau[6], J.E. Turney[19], E. Tzamariudaki[25], S. Udluft[25], A. Usik[24],

S. Valkár[30], A. Valkárová[30], C. Vallée[22], P. Van Mechelen[4], Y. Vazdik[24], S. von Dombrowski[37], K. Wacker[7], R. Wallny[37], T. Walter[37], B. Waugh[21], G. Weber[11], M. Weber[14], D. Wegener[7], A. Wegner[25], T. Wengler[13], M. Werner[13], G. White[17], S. Wiesand[33], T. Wilksen[10], M. Winde[35], G.-G. Winter[10], C. Wissing[7], M. Wobisch[2], H. Wollatz[10], E. Wünsch[10], A.C. Wyatt[21], J. Žáček[30], J. Zálešák[30], Z. Zhang[26], A. Zhokin[23], F. Zomer[26], J. Zsembery[9] and M. zur Nedden[10]

[1] I. Physikalisches Institut der RWTH, Aachen, Germany[a]
[2] III. Physikalisches Institut der RWTH, Aachen, Germany[a]
[3] School of Physics and Space Research, University of Birmingham, Birmingham, UK[b]
[4] Inter-University Institute for High Energies ULB-VUB, Brussels; Universitaire Instelling Antwerpen, Wilrijk; Belgium[c]
[5] Rutherford Appleton Laboratory, Chilton, Didcot, UK[b]
[6] Institute for Nuclear Physics, Cracow, Poland[d]
[7] Institut für Physik, Universität Dortmund, Dortmund, Germany[a]
[8] Joint Institute for Nuclear Research, Dubna, Russia
[9] DSM/DAPNIA, CEA/Saclay, Gif-sur-Yvette, France
[10] DESY, Hamburg, Germany[a]
[11] II. Institut für Experimentalphysik, Universität Hamburg, Hamburg, Germany[a]
[12] Max-Planck-Institut für Kernphysik, Heidelberg, Germany[a]
[13] Physikalisches Institut, Universität Heidelberg, Heidelberg, Germany[a]
[14] Kirchhoff-Institut für Physik, Universität Heidelberg, Heidelberg, Germany[a]
[15] Institut für experimentelle und angewandte Physik, Universität Kiel, Kiel, Germany[a]
[16] Institute of Experimental Physics, Slovak Academy of Sciences, Košice, Slovak Republic[e,f]
[17] School of Physics and Chemistry, University of Lancaster, Lancaster, UK[b]
[18] Department of Physics, University of Liverpool, Liverpool, UK[b]
[19] Queen Mary and Westfield College, London, UK[b]
[20] Physics Department, University of Lund, Lund, Sweden[g]
[21] Department of Physics and Astronomy, University of Manchester, Manchester, UK[b]
[22] CPPM, CNRS/IN2P3 - Univ Mediterranee, Marseille - France
[23] Institute for Theoretical and Experimental Physics, Moscow, Russia
[24] Lebedev Physical Institute, Moscow, Russia[e,h]
[25] Max-Planck-Institut für Physik, München, Germany[a]
[26] LAL, Université de Paris-Sud, IN2P3-CNRS, Orsay, France
[27] LPNHE, École Polytechnique, IN2P3-CNRS, Palaiseau, France
[28] LPNHE, Universités Paris VI and VII, IN2P3-CNRS, Paris, France
[29] Institute of Physics, Academy of Sciences of the Czech Republic, Praha, Czech Republic[e,i]
[30] Faculty of Mathematics and Physics, Charles University, Praha, Czech Republic[e,i]
[31] INFN Roma 1 and Dipartimento di Fisica, Università Roma 3, Roma, Italy
[32] Paul Scherrer Institut, Villigen, Switzerland
[33] Fachbereich Physik, Bergische Universität Gesamthochschule Wuppertal, Wuppertal, Germany[a]
[34] Yerevan Physics Institute, Yerevan, Armenia
[35] DESY, Zeuthen, Germany[a]
[36] Institut für Teilchenphysik, ETH, Zürich, Switzerland[j]
[37] Physik-Institut der Universität Zürich, Zürich, Switzerland[j]

[38] Present address: Institut für Physik, Humboldt-Universität, Berlin, Germany
[39] Also at Rechenzentrum, Bergische Universität Gesamthochschule Wuppertal, Wuppertal, Germany
[40] Also at Institut für Experimentelle Kernphysik, Universität Karlsruhe, Karlsruhe, Germany
[41] Also at Dept. Fis. Ap. CINVESTAV, Mérida, Yucatán, México[k]
[42] Also at University of P.J. Šafárik, Košice, Slovak Republic
[43] Also at CERN, Geneva, Switzerland

[†] Deceased

[a] Supported by the Bundesministerium für Bildung, Wissenschaft, Forschung und Technologie, FRG, under contract numbers 7AC17P, 7AC47P, 7DO55P, 7HH17I, 7HH27P, 7HD17P, 7HD27P, 7KI17I, 6MP17I and 7WT87P
[b] Supported by the UK Particle Physics and Astronomy Research Council, and formerly by the UK Science and Engineering Research Council
[c] Supported by FNRS-FWO, IISN-IIKW
[d] Partially Supported by the Polish State Committee for Scientific Research, grant No. 2P0310318 and SPUB/DESY/P-03/DZ 1/99
[e] Supported by the Deutsche Forschungsgemeinschaft
[f] Supported by VEGA SR grant no. 2/5167/98
[g] Supported by the Swedish Natural Science Research Council
[h] Supported by Russian Foundation for Basic Research grant no. 96-02-00019
[i] Supported by GA AVČR grant number no. A1010821
[j] Supported by the Swiss National Science Foundation
[k] Supported by CONACyT

1 Introduction

A large contribution to the photoproduction of J/ψ mesons is the *elastic* process, $\gamma\, p \to J/\psi\, p$, which has been studied previously over a wide range, from threshold up to a photon-proton centre-of-mass energy, $W_{\gamma p}$, of approximately 160 GeV in ep collisions at HERA. The cross section for elastic J/ψ photoproduction was observed to rise much more steeply with $W_{\gamma p}$ [1–4] than that for the light vector mesons [5]. In perturbative quantum chromodynamics (pQCD), the process is viewed as an almost real photon from the lepton coupling to a pair of $c\overline{c}$ quarks which interact with the proton via exchange of two (or more) gluons and evolve into a J/ψ meson. The cross section is then proportional to the square of the gluon density of the proton. The rapid rise of the gluon density at low fractional gluon momenta leads to the observed rise of the cross section with $W_{\gamma p}$ [6–8]. In such calculations, the heavy quark mass serves as the QCD scale. Therefore, it is of interest to measure the cross section of the Υ meson, for which perturbation theory might be more reliable. In non-perturbative models, J/ψ production has been described in terms of pomeron exchange [9, 10]. Since the standard soft pomeron fails to describe inclusive electroproduction and the observed $W_{\gamma p}$ dependence of the J/ψ cross section, extensions of such models have been proposed [11]. In one such extension [12], which is compared to the data of this paper, an extra "hard" pomeron is introduced.

Here, we present new data obtained by the H1 experiment which may lead to a better understanding of the elastic production process. The $W_{\gamma p}$ dependence of the cross section for elastic J/ψ photoproduction is measured, with increased statistics in an enlarged range of $26 \leq W_{\gamma p} \leq 285$ GeV, and compared to QCD and pomeron models. Furthermore, the differential cross section $d\sigma/dt$, where $|t|$ is the squared four-momentum transfer to the proton, is measured as a function of t and of $W_{\gamma p}$. From its $W_{\gamma p}$ dependence, an effective Regge trajectory is determined using data from this experiment alone, thus avoiding relative normalization problems when comparing data from different experiments. The results are compared to the predictions of the two-pomeron model [12] and also to a recent calculation in next-to-leading order (NLO) using the BFKL equation [13]. Finally, we present a measurement of elastic photoproduction of Υ mesons which allows a test of the predictions of pQCD at a higher mass scale [14, 15].

2 Data Analysis

We report, here, an analysis of the process $ep \to eVp$, ($V = J/\psi$ or Υ), where J/ψ mesons decaying to $\mu^+\mu^-$ and e^+e^- and $\Upsilon \to \mu^+\mu^-$ are observed. The data were taken with the H1 detector while HERA was operating with positrons of 27.5 GeV and protons of 820 GeV.

The kinematics of an ep reaction are described by the square of the ep centre-of-mass energy $s = (p + k)^2$, the squared four-momentum transfer from the positron $Q^2 = -q^2 = -(k - k')^2$ and the scaled energy transfer $y = (p{\cdot}q)/(p{\cdot}k)$, where k, k', p and q are the four-momenta of the incident and scattered positron, the incoming proton and the exchanged photon, respectively. In the photoproduction domain $Q^2 \to 0$, the positron is scattered at small angles and generally not observed. In the present analysis, the photoproduction region is defined by $Q^2 \leq 1\,\mathrm{GeV}^2$. The average Q^2 values, derived from the Monte Carlo simulation, are $\langle Q^2 \rangle \simeq 0.05\,\mathrm{GeV}^2$ for

the J/ψ analyses and $\langle Q^2 \rangle \simeq 0.11\,\mathrm{GeV}^2$ for the Υ analysis. In the photoproduction limit, the square of the centre-of-mass energy of the photon-proton system $W^2_{\gamma p} = (p+q)^2$ is given by $W^2_{\gamma p} \simeq ys$. It is calculated from the relation: $y = (E - p_z)_V/(2\,E_e)$, where E and p_z denote the total energy and longitudinal component[1] of the momentum of the vector meson V and E_e is the energy of the incident positron.

Detector and Data Selection

The H1 detector is described in detail elsewhere [16]. The main detector consists of a system of drift and proportional chambers: the central track detector (CTD), covering the polar angle range $15^\circ \lesssim \theta \lesssim 165^\circ$ and the forward track detectors (FTD), covering $7^\circ \lesssim \theta \lesssim 25^\circ$. The tracking detectors are surrounded by a liquid argon calorimeter (LAr, $4^\circ \lesssim \theta \lesssim 154^\circ$), a scintillating fibre calorimeter (spaghetti calorimeter, SpaCal [17], $153^\circ \lesssim \theta \lesssim 178^\circ$) and an instrumented iron return yoke (central muon detector, CMD, $4^\circ \lesssim \theta \lesssim 171^\circ$). The interaction region is surrounded by an assembly of high precision silicon detectors, the backward part of which (backward silicon tracker, BST [18]) is used in this analysis. The BST, which became fully operational in 1997, is a four plane silicon strip detector telescope arranged concentrically around the beam axis to measure the polar angle of tracks ($172^\circ \lesssim \theta \lesssim 176.5^\circ$).

Electrons are identified in the LAr or the SpaCal calorimeters. Muons are identified in the LAr calorimeter, in the CMD and, at small polar angles, in the forward muon detector (FMD, $3^\circ \lesssim \theta \lesssim 17^\circ$), which consists of drift chambers on either side of a toroidal magnet. The momentum and angular measurements of the decay leptons are provided by the CTD (FTD) in the central (forward) detector region. At the highest values of $W_{\gamma p}$, both electrons are scattered into SpaCal. In this case, the polar angle and the event vertex are derived from track measurements in the BST.

In elastic photoproduction of J/ψ and Υ mesons, both the scattered positron and the scattered proton are not generally detected. The largest background is due to processes in which the proton dissociates to form a hadronic state Y, the proton remnant. To reject such events, the so-called "forward detectors" are utilized: the proton remnant tagger, PRT, scintillation counters covering polar angles close to the proton beam, the drift chambers of the FMD in front of the toroid and the forward part of the LAr calorimeter ($\theta \leq 10^\circ$). Proton remnants with masses $M_Y \gtrsim 1.6$ GeV can be detected.

The experimental signature of the process $e\,p \to e\,V\,p$, $V \to \ell^+\ell^-$ in the photoproduction domain is a pair of leptons in an otherwise "empty" detector. The data selection thus requires only two decay leptons to be observed in the main detector with no signal in the forward detectors. The value of $W_{\gamma p}$ is related to the polar angles of the vector meson and therefore also to the polar angle of the decay leptons. Selection criteria are used which correspond to different detector regions and ranges of $W_{\gamma p}$ (see Table 1). For each analysis region, the decay mode, $\mu^+\mu^-$ or e^+e^-, with the better detection efficiency is chosen.

In the central region, $J/\psi \to \mu^+\mu^-$ is analysed in the range $40 \leq W_{\gamma p} \leq 150$ GeV. Exactly two oppositely charged particles, measured in the CTD, are required with transverse momenta

[1] The forward ($+z$) direction, with respect to which polar angles are measured, is defined as that of the incident proton beam direction.

	Central region		Backward region		Forward region
Decay channel	$J/\psi \to \mu^+\mu^-$	$\Upsilon \to \mu^+\mu^-$	$J/\psi \to e^+e^-$		$J/\psi \to \mu^+\mu^-$
$\langle Q^2 \rangle$ [GeV^2]	0.05	0.11	0.05		0.05
Lepton polar angle region [°]	$20-160$	$20-165$	$80-155$ $155-176$	$155-175.5$ $155-174$	$8-16$ $20-160$
$W_{\gamma p}$ range [GeV]	$40-150$	$70-250$	$135-210$	$210-285$	$26-36$
Data from	$1996-97$	$1994-97$	$1996-97$	1997	$1996-97$
$\int \mathcal{L}$ dt [pb^{-1}]	20.5	27.5	20.5	10.0	20.5

Table 1: *Summary of the different data sets.*

(with respect to the beamline) $p_t > 0.8$ GeV. At least one of these must be validated as a muon in the LAr calorimeter or in the CMD (for further details see [1, 3, 19]). Background from cosmic ray muons is rejected by an acolinearity cut. Triggers based on muon and track signatures from the decay leptons are used. For the reconstruction of Υ decays, the acceptance region is $70 \leq W_{\gamma p} \leq 250$ GeV. In order to optimize the signal to background ratio, both muons must be identified and a tighter cut against cosmic rays is applied.

For the J/ψ analysis in the backward region, the decay to electrons is used. Two sets of selection criteria are applied, depending on the event kinematics. The first set ($135 < W_{\gamma p} < 210$ GeV) requires one decay electron to be measured in the CTD and one in the SpaCal calorimeter. The electron measured in the CTD must have a momentum $p > 0.8$ GeV and a transverse momentum $p_t > 0.7$ GeV. It is validated by an electromagnetic cluster in the LAr calorimeter. The other electron is selected by requiring a cluster in the SpaCal calorimeter with energy above 4.2 GeV, which is assumed to originate from the intersection of the first electron track with the z-axis. In order to suppress inelastic contributions and background, no further tracks are allowed and any energy in the SpaCal outside the selected electron cluster must be below $6\,\%$ of its energy. The second selection ($210 < W_{\gamma p} < 285$ GeV) requires both electrons to be detected in the SpaCal calorimeter as described above. They must be validated either by hits in a proportional chamber or by a track in the BST. By requiring two charged particles, at least one of which is in the acceptance of the BST, most of the non-resonant background from the QED process $ep \to e\gamma p$ is rejected. The triggers for both selections are based on signals from the SpaCal and the CTD. In addition the triggers in the central and backward regions use a trigger based on neural networks [20].

In the J/ψ analysis in the forward region ($26 \leq W_{\gamma p} \leq 36$ GeV), the FMD is used to identify one decay muon with momentum above 5 GeV. The other muon is measured in the CTD with momentum above 0.8 GeV. No other tracks, except those associated with the muons, are allowed. Proton dissociative events are rejected by a forward detector analysis, taking into account that one of the muons passes through the drift chambers of the FMD and may pass through the forward part of the LAr calorimeter. The FMD also supplies the trigger for these events in conjunction with signals from track chambers and the central muon detector.

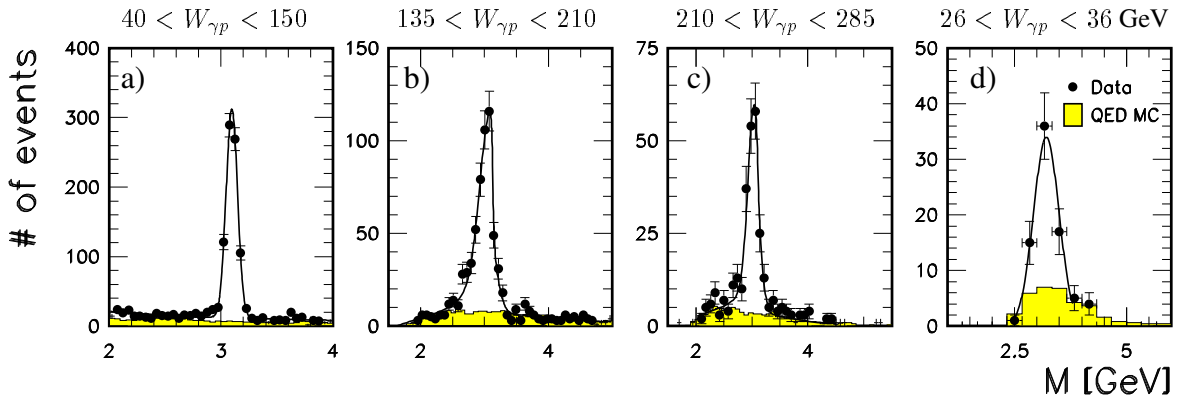

Figure 1: *Mass spectra for the four $W_{\gamma p}$ regions of the elastic J/ψ selection: a) $\mu^+\mu^-$ pairs in the central region, b) and c) e^+e^- pairs in the backward region, d) $\mu^+\mu^-$ pairs in the forward region. A fit of the signal region as described in the text (full line) and the simulated mass spectra from QED background processes (shaded histograms) are shown.*

Cross Section Determination

After the data selection, clear peaks at the J/ψ mass are observed in the distributions of the invariant mass of the two leptons in all analysis regions (Figure 1). The remaining background in the forward and central regions is dominated by the process $\gamma\gamma \to \mu^+\mu^-$, where the photons originate from both the positron and proton. In the backward region at very high $W_{\gamma p}$, the background is composed of the processes $\gamma\gamma \to e^+e^-$ and $ep \to e\gamma p$, where the photon and electron are scattered at large angles. These background processes can be simulated by the LPAIR [21] and COMPTON [22] generators, respectively.

The number of J/ψ events in the central region (Figure 1a) is determined in each analysis bin by a fit which uses a Gaussian for the signal and a polynomial for the background. In the backward region ($J/\psi \to e^+e^-$), the number of events is determined by fitting the signal region with a Gaussian and an exponential to describe the low mass tail, and subtracting the simulated background (Figure 1b,c). The low mass tail is caused by radiative effects in the the detector material. In the forward region, the background is determined by the Monte Carlo simulation.

For the calculation of the cross section, the number of events without a signal in the forward detectors is corrected for acceptance and efficiency losses by using the Monte Carlo simulation DIFFVM [23]. DIFFVM is based on the Vector Meson Dominance Model and Regge phenomenology. Either the elastic or the proton dissociative processes can be generated. The Q^2, $W_{\gamma p}$ and t dependences have been adjusted to fit the data.

A correction is applied for the remaining background from proton dissociation which is typically $10 - 13\%$ in the central and backward regions and 30% in the forward region. It is determined from the Monte Carlo simulation and cross checked with data samples with and without signals in the forward detectors. The non-prompt J/ψ events from $\psi(2S)$ decays ($\sim 3\%$) are subtracted according to their measured cross section [24] and branching ratio [25]. The total efficiencies (including acceptance) for the J/ψ analyses are typically 5%, 14% and 20% in the forward, central and backward regions, respectively. The trigger efficiencies are about 18%, 20% and $38 - 60\%$, depending on $W_{\gamma p}$. At the highest $W_{\gamma p}$ values ($W_{\gamma p} \gtrsim 200$ GeV), the

trigger efficiency is 100%, within errors. The losses in this region are mainly due to the limited acceptance.

The ep cross section is obtained using the measured luminosity and the branching ratio of the J/ψ decay to electrons or muons, $(6.0 \pm 0.2)\%$ [25] each. For the decay to electrons, the radiative decay $J/\psi \rightarrow e^+e^-\gamma$ with the branching ratio $(0.88 \pm 0.14)\%$ [25] is also taken into account. The photoproduction cross section is calculated from the electroproduction cross section, assuming factorization of the ep reaction into emission of photons, described by a photon flux (Weizsäcker-Williams approximation [26]), followed by a γp reaction.

The systematic error for the J/ψ analysis in the central region increases with $W_{\gamma p}$ from 11% to 14% with an estimated correlated part, which affects only the normalization, of $5-6\%$. The largest contributions are the uncertainties in the determination of the proton dissociative background ($5-10\%$), the efficiency of the lepton identification (6.5%) and the trigger efficiency (6%). In the backward region, the systematic uncertainties are estimated to be, on average, 16%. For $W_{\gamma p} \lesssim 200$ GeV, the contributions are similar to those in the central region. For $W_{\gamma p} \gtrsim 200$ GeV, the main contributions are due to the uncertainties in the subtraction of the residual background from QED processes (10%) and proton dissociation (10%). In the forward region (low $W_{\gamma p}$), the total uncertainty is 26%, where the largest contributions are the uncertainty of the trigger efficiency (18%) and the determination of the background (16%).

Radiative corrections have been neglected throughout the analysis. Recent calculations for elastic photoproduction of ρ mesons [27] suggest that, for J/ψ photoproduction, they are small compared to experimental errors.

3 $W_{\gamma p}$ Dependence of J/ψ Production

The cross section for elastic photoproduction of J/ψ mesons, as a function of $W_{\gamma p}$, is listed in Table 2 and is shown in Figure 2a, together with previous H1 and ZEUS results [1,2]. The data show good agreement in the region of overlap. A fit of the form $W_{\gamma p}^{\delta}$ to the present H1 data between 26 and 285 GeV yields a value of $\delta = 0.83 \pm 0.07$ (including statistical and systematic errors). This result confirms, with smaller errors, the steep rise of the J/ψ cross section with $W_{\gamma p}$ observed previously [1,2], which is much larger than for the light vector mesons [5].

In Figure 2a, the HERA data are shown with predictions from a leading order pQCD calculation [7,8] using various gluon density distributions. The important prediction concerns the $W_{\gamma p}$ dependence of the cross section since the absolute magnitude is more dependent on a number of parameters and on non-perturbative effects. The slope of the data is described well using either the gluon density CTEQ4M [28] or MRSR2 [29] while the GRV-HO [30] based result is too steep.

For the comparison with models based on pomeron exchange, the present data, previous HERA data and results from fixed-target experiments [31][2] are used (Figure 2b). A pomeron trajectory of the form $\alpha(t) = \alpha_0 + \alpha' t$ leads to a $W_{\gamma p}$ dependence $\sigma_{\gamma p} \propto W_{\gamma p}^{4(\alpha_0-1)}/b(\alpha', \ln W_{\gamma p})$

[2] Only fixed-target results are shown which were performed on H_2 or D_2 targets and which have been corrected for contributions from proton dissociative processes.

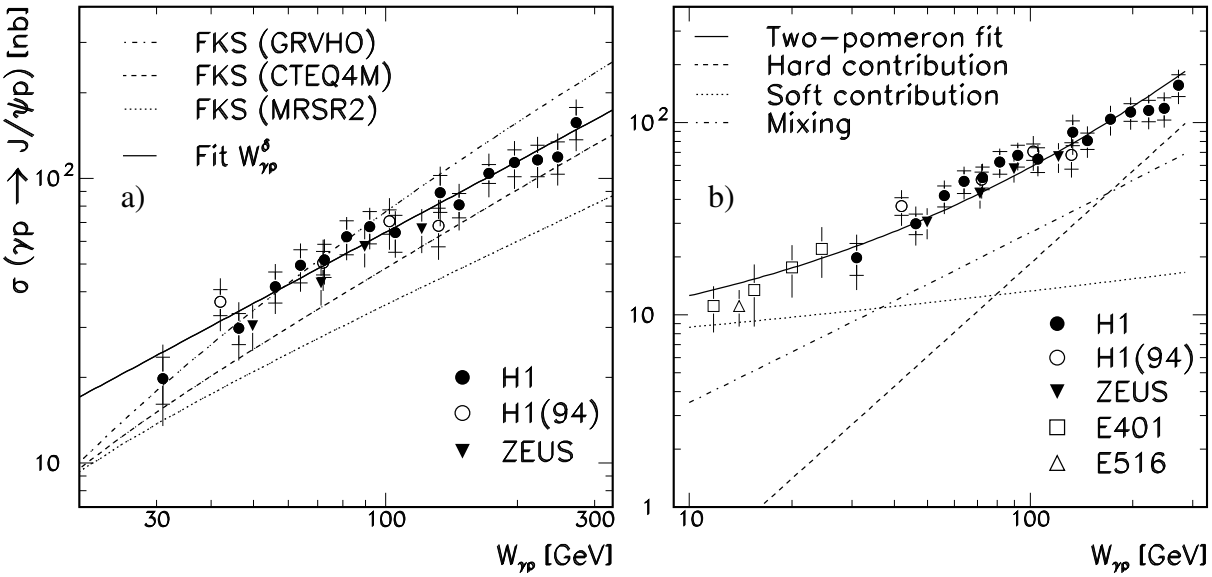

Figure 2: *a) The cross section $\sigma(\gamma p \to J/\psi p)$ versus $W_{\gamma p}$ from this analysis and previous HERA results. The inner and outer error bars show the statistical and total errors, respectively. The full line represents a fit of the form $\sigma_{\gamma p} \propto W_{\gamma p}^{\delta}$ to the present H1 data, yielding $\delta = 0.83 \pm 0.07$ with a $\chi^2/dof = 4.6/13$. QCD predictions by Frankfurt et al. [8] using various parameterizations of the gluon density in the proton and the charm quark mass of 1.48 GeV as chosen in [8] are also shown. b) The same HERA data as in a) and results from fixed-target experiments with a fit of the two-pomeron model by Donnachie and Landshoff (full line; $\chi^2/dof = 16.1/22$). Only the contributions of the soft and hard pomeron amplitudes were adjusted allowing for mixing [12]. The separate contributions are indicated.*

[9, 10]. The parameters of the established soft and the proposed hard pomeron trajectories are $(\alpha_0, \alpha')_{\text{soft}} = (1.08, 0.25\,\text{GeV}^{-2})$ and $(\alpha_0, \alpha')_{\text{hard}} = (1.418, 0.1\,\text{GeV}^{-2})$ [12]. By using these trajectories and fitting the relative contributions and mixing as defined in [12], a good representation of the data is given. The relative contributions of hard, soft and mixing terms are found to vary between 0.1 : 0.5 : 0.4 at $W_{\gamma p}$= 30 GeV and 0.5 : 0.1 : 0.4 at $W_{\gamma p}$= 250 GeV.

4 Differential Cross Section $d\sigma/dt$ for J/ψ Mesons

The dependence of the photoproduction cross section of J/ψ mesons on t is studied in the region of $40 \leq W_{\gamma p} \leq 150$ GeV, which provides good t resolution. First, this dependence is measured averaging over the entire $W_{\gamma p}$ range, assuming an exponential behaviour. Then, the dependence of $d\sigma/dt$ on $W_{\gamma p}$ in fixed t bins is determined and an effective Regge trajectory is derived.

***t* Distribution:** The variable t is approximated by $t \simeq -(\vec{p}_t)^2$, where $\vec{p}_t$ is the transverse momentum of the J/ψ meson. The resolution of t, obtained from the Monte Carlo simulation of vector mesons, is typically 0.035 GeV^2 and increases to 0.060 GeV^2 for $|t| \approx 1.2$ GeV^2. The events without a signal in the forward detectors, in the mass range $2.9 \leq M_{\mu\mu} \leq 3.3$ GeV,

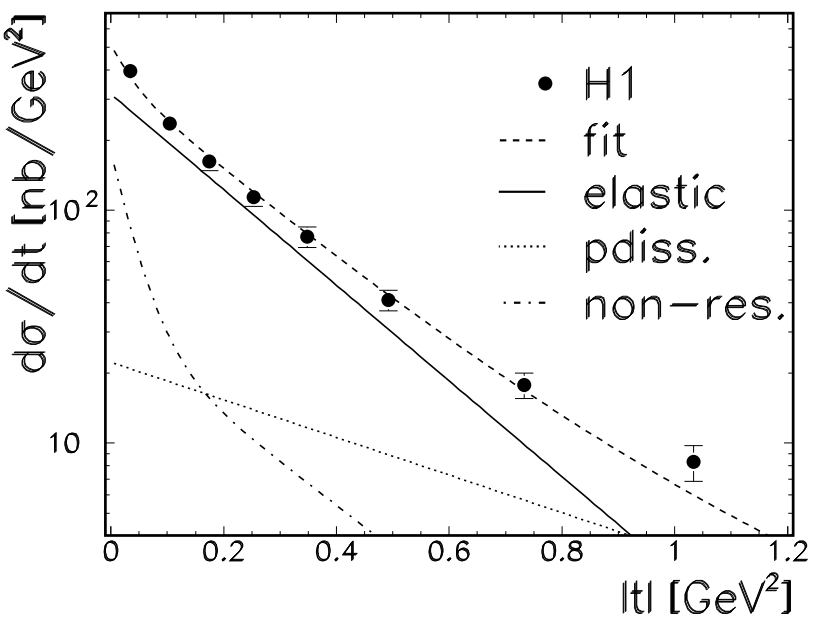

Figure 3: *The differential cross section $d\sigma/dt$ for elastic J/ψ photoproduction, as a function of $|t|$, averaged over the energy region $40 \leq W_{\gamma p} \leq 150$ GeV. Only statistical errors are given. Also shown is the result of a fit (dashed line; $\chi^2/dof = 4.7/6$) to the data which includes the three different contributions described in the text. The solid curve shows the fit result for elastic J/ψ production assuming an exponential t dependence.*

are divided into bins in t and corrected for efficiencies but not for remaining backgrounds. Photon-proton cross sections are calculated as described in section 2, yielding the resulting values of $d\sigma/dt$ shown in Figure 3.

With this selection, the data contain elastic J/ψ events (81%), events with proton dissociation (13%) and non-resonant background (6%). These fractions result from the analysis described in section 2 and are fixed in the subsequent analysis of the t-dependence. The t-dependence of the proton dissociative J/ψ contribution is obtained by fitting those corrected data which contain a signal in the forward detectors with one exponential function. The different t dependence of the efficiencies for proton dissociative events with and without signals in the forward detectors is taken into account. The non-resonant background is described by a sum of two exponential functions which are obtained by fitting the data outside of the J/ψ mass region.

A common fit of the three contributions to the data is then carried out, assuming an exponential distribution $e^{-b|t|}$ for the elastic cross section (see Figure 3). The only free parameters in this fit are the elastic slope parameter b and an overall normalization. Only the statistical errors of the data are taken into account in the fit. A value $b = (4.73 \pm 0.25^{+0.30}_{-0.39})$ GeV^{-2} is derived for $|t| \leq 1.2$ GeV^2, where the first error is statistical. The systematic uncertainty is obtained by varying the data selection cuts, the t distribution of the generated events for both the acceptance and efficiency corrections and the admixture of the background contributions (both relative normalizations and shapes). The resulting value of b agrees within errors with the previous H1 result [1] and with a similar result from the ZEUS collaboration [2].

Regge Trajectory: In the description of elastic scattering based on Regge phenomenology and pomeron exchange, the energy dependence of the elastic cross section follows a power law:

$$\frac{d\sigma}{dt} = \left.\frac{d\sigma}{dt}\right|_{t=0, W_{\gamma p}=W_0} \cdot e^{-b_0|t|} \left(\frac{W_{\gamma p}}{W_0}\right)^{4(\alpha(t)-1)}, \tag{1}$$

where $\alpha(t) = \alpha_0 + \alpha' t$ denotes the exchanged trajectory and b_0 and W_0 are constant parameters not determined by the theory. Whereas Regge theory predicts a change of the $W_{\gamma p}$ dependence with t, there is no such simple relationship in pQCD [7].

In order to determine the effective trajectory $\alpha(t)$ in elastic J/ψ production, the data used for Figure 3 are analysed as functions of $W_{\gamma p}$ and t. The data are divided into five bins in t and six bins in $W_{\gamma p}$. According to the Monte Carlo simulation, the migrations due to resolution effects range from $20-50\%$ in t and are negligible in $W_{\gamma p}$. The differential cross section $d\sigma/dt$ is determined in each bin (t_i, W_j), as described in section 2, i.e. correcting for non resonant and proton dissociative background. The resulting values are listed in Table 3 and shown in Figure 4 as functions of $W_{\gamma p}$ in the five t bins. Statistical and systematic errors, excluding the contributions which affect only the normalization, are taken into account; the statistical errors

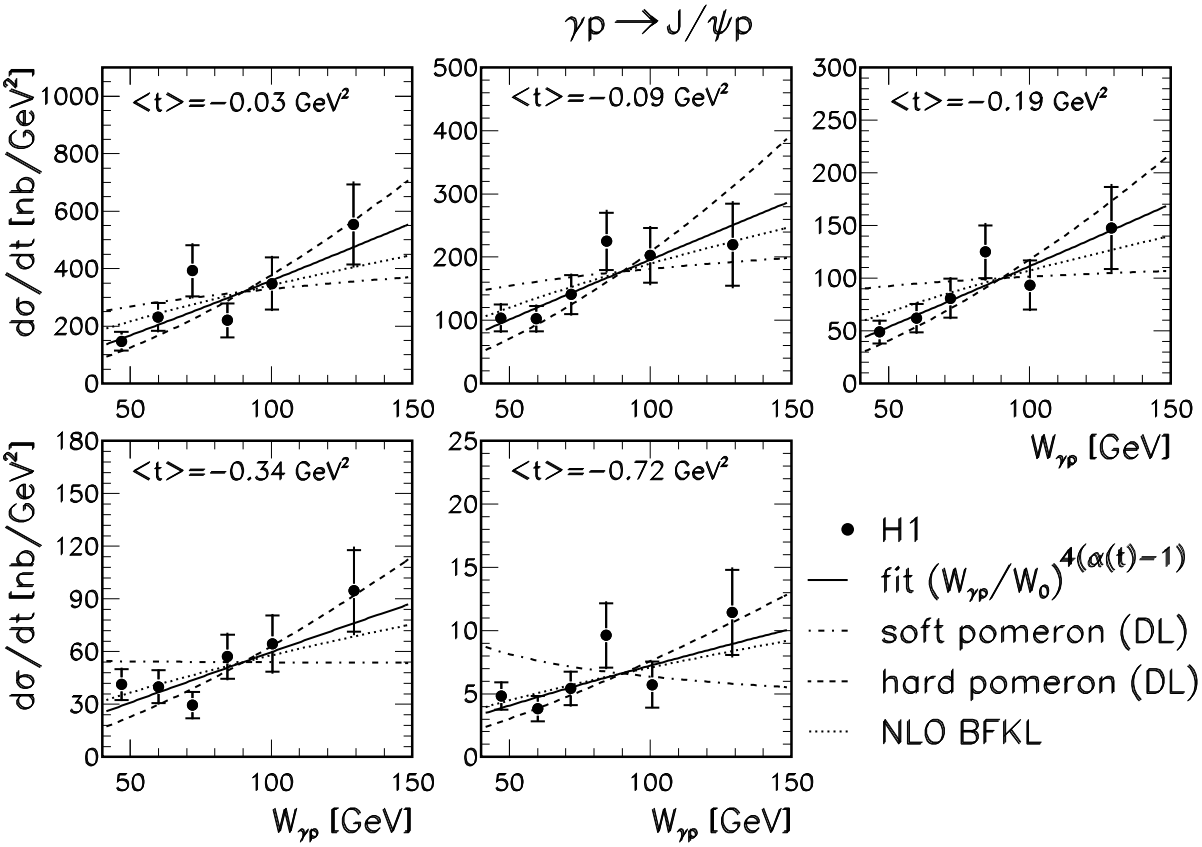

Figure 4: *The differential cross section $d\sigma/dt$ as a function of $W_{\gamma p}$ in five bins of t together with a fit of the form $d\sigma/dt = N \cdot (W_{\gamma p}/W_0)^{4(\alpha(t)-1)}$ (solid line). The inner error bars on the data points show the dominating statistical errors and the outer bars the total error. The predictions of the soft and hard Donnachie-Landshoff pomeron trajectories [12] are shown as dash-dotted and dashed lines. The prediction based on a NLO BFKL calculation [13] is given as a dotted line. All theoretical curves are normalized to the fit at $W_0 = 90$ GeV.*

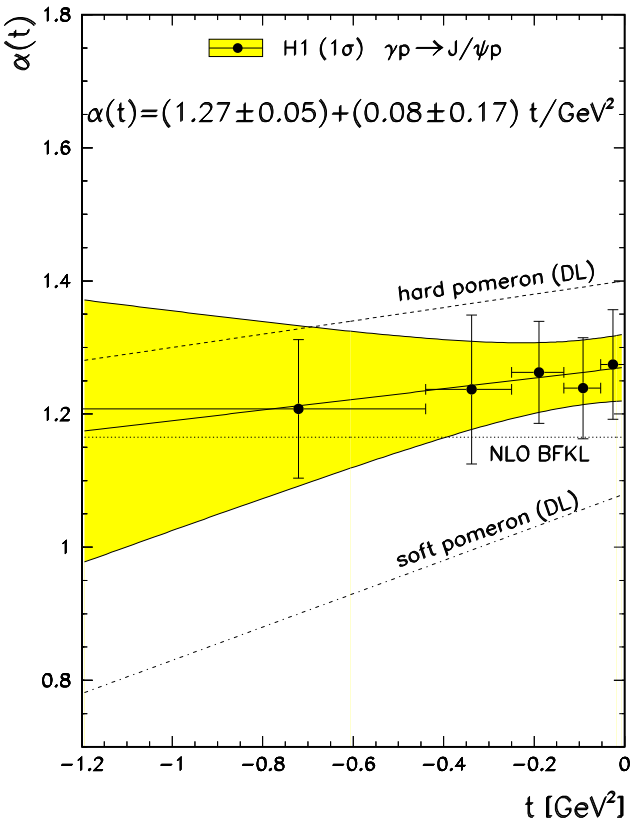

Figure 5: *The measured Regge trajectory $\alpha(t) = \alpha_0 + \alpha' t$ for the process $\gamma p \to J/\psi\, p$. The solid line shows the result of the fit. The one standard deviation contour is indicated by a shaded band. Also shown are the soft and the hard Donnachie-Landshoff pomeron trajectories [12] and a result based on a NLO BFKL calculation [13].*

dominate. The data in each bin t_i are fitted as a function of $W_{\gamma p}$ (Equation 1) with $\alpha(t_i)$ and a normalization constant as free parameters.

The results of these fits are shown as full lines in Figure 4. The respective curves, corresponding to the soft and the hard pomeron trajectories by Donnachie and Landshoff [12] as well as a hard pomeron extracted from a NLO BFKL calculation [13], are also shown. Note that the differential cross section $d\sigma/dt$ at fixed t exhibits a rise with $W_{\gamma p}$ at all t values, in contrast to the expectation from the soft pomeron model.

The resulting fit values of $\alpha(t_i)$ are shown as points in Figure 5; the error bars contain the statistical and systematic uncertainties. A fit to these values of the form $\alpha(t) = \alpha_0 + \alpha' t$, where α_0 and α' are free parameters, yields the result

$$\alpha(t) = (1.27 \pm 0.05) + (0.08 \pm 0.17) \cdot t/\mathrm{GeV}^2.$$

This fit is shown in Figure 5, including a band which reflects the one standard deviation uncertainty, taking into account correlations between α_0 and α'. The resulting effective trajectory lies, as expected from the analysis of the total cross section (see Figure 2a), in between the soft and the hard pomeron trajectories of Donnachie and Landshoff. A prediction for a pomeron,

derived from a NLO BFKL calculation [13], is also shown in Figure 5. Note, however, that in this calculation only α_0 is predicted[3] and $\alpha' = 0$ is assumed for the plot. The measured intercept α_0 in J/ψ production is found to be significantly larger than in the production of the light vector mesons ρ and ϕ. The slope α' is found to be compatible with zero, in contrast to the value measured for ρ and ϕ mesons [32]. The present results allow, for the first time, the extraction of the effective Regge trajectory exchanged in J/ψ photoproduction from a single experiment, avoiding relative normalization uncertainties between experiments. A previous fit [33], using earlier HERA results and fixed target data at lower $W_{\gamma p}$, gives compatible results.

5 Υ Production

The mass distribution of the selected di-muon events, without a signal in the forward counters, is shown in Figure 6a. An excess of events is visible at a mass of ~ 9.4 GeV above a background which is fitted by a power law. The background is, within errors, described by the process $\gamma\gamma \to \mu^+\mu^-$. The significance of the excess is about two standard deviations and its position is compatible with these events arising from $\Upsilon(1S)$ decay. The mass resolution is $\sigma \sim 250$ MeV. Due to limited statistics, small contributions from the two lowest radial excitations $\Upsilon(2S)$ and $\Upsilon(3S)$ cannot be excluded. In order to estimate the number of signal events, a wide mass interval is chosen which extends from $2\,\sigma$ below the $\Upsilon(1S)$ to $2\,\sigma$ above the $\Upsilon(3S)$ state ($8.9 \lesssim m_{\mu\mu} \lesssim 10.8$ GeV). Subtracting the background, 12.2 ± 6.3 signal events are obtained. Corrections for the remaining background, due to diffractive proton dissociation (16%) and the total selection and trigger efficiency (24%), are determined from the Monte Carlo simulation, cross checked with data similarly to the J/ψ analysis. Taking into account the total integrated luminosity and using the Weizsäcker-Williams approximation [26], a γp cross section in the range $70 \leq W_{\gamma p} \leq 250$ GeV with an average value of $\langle W_{\gamma p} \rangle = 143$ GeV is obtained:

$$\sigma(\gamma\, p \to \Upsilon\, p) \times \mathrm{BR}(\Upsilon \to \mu^+\mu^-) = (19.2 \pm 9.9 \pm 4.8)\ \mathrm{pb},$$

where Υ includes the states $\Upsilon(1S)$, $\Upsilon(2S)$ and $\Upsilon(3S)$. The first error is statistical and the second systematic (25%). The latter is calculated by varying the definition of the signal and background regions, using different estimates of the background function or calculating the background from the $\gamma\gamma \to \mu^+\mu^-$ prediction and taking into account uncertainties of efficiencies.

In order to extract the cross section for the production of the $\Upsilon(1S)$ state, an assumption must be made about its relative production ratio. We choose a fraction of 70%. This is in broad agreement with an estimate using the branching ratios and the electronic widths of the different Υ states [25] and with a recent calculation [14]. Using the standard branching ratios for $\Upsilon(1S)$, $\Upsilon(2S)$ and $\Upsilon(3S)$ [25], the result for the elastic $\Upsilon(1S)$ photoproduction cross section is

$$\sigma(\gamma p \to \Upsilon(1S)p) = (0.55 \pm 0.28 \pm 0.14)\ \mathrm{nb}\,.$$

In Figure 6 b), the measured cross section $\sigma(\gamma p \to \Upsilon(1S)p)$ is shown together with the ZEUS measurement [34], which agrees well with our result. Recent pQCD calculations [14, 15] are

[3] We chose the solution corresponding to $\xi = 3$ in Table 2 of [13].

able to describe the data after consideration of two effects: the real part of the scattering amplitude and the non-diagonal parton distributions in the proton. Such effects are found to be more important for the production of the Υ than for the J/ψ meson, due to its larger mass.

6 Summary

Improved results over an extended kinematic range on the elastic photoproduction of J/ψ mesons are presented. The total photoproduction cross section is measured as a function of the photon-proton centre-of-mass energy $W_{\gamma p}$ in the range $26 \leq W_{\gamma p} \leq 285$ GeV, where it can be parameterized as $\sigma_{\gamma p} \propto W_{\gamma p}^{\delta}$ with $\delta = 0.83 \pm 0.07$.

The data are well described by a perturbative QCD calculation by Frankfurt et al. [8], where a good description is obtained using the CTEQ4M or MRSR2 gluon densities in the proton. The data in this $W_{\gamma p}$ range can also be described by a non-perturbative model which assumes the exchange of two pomeron trajectories. However, a model with only a soft pomeron is ruled out.

The differential cross section, $d\sigma/dt$, for elastic J/ψ production, averaged over the range $40 \leq W_{\gamma p} \leq 150$ GeV, is well described by a single exponential for the accessible range below $|t| = 1.2$ GeV^2 with a slope parameter $b = (4.73 \pm 0.25^{+0.30}_{-0.39})$ GeV^{-2}.

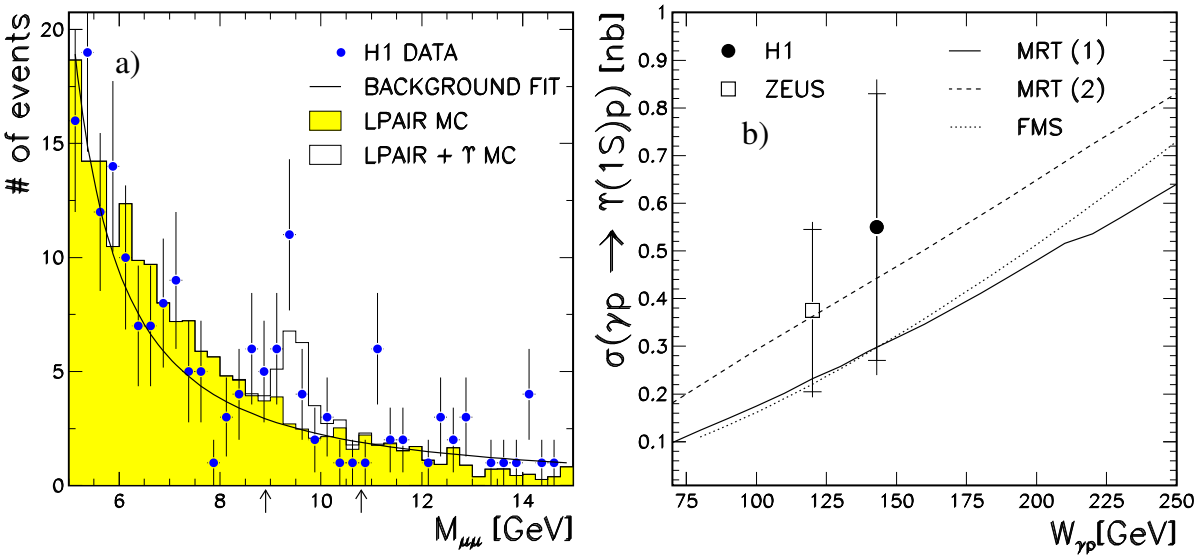

Figure 6: *a) The invariant mass spectrum of the selected di-muon events without a signal in the forward detectors. The solid line shows the result of a fit to the background region. The histograms are Monte Carlo predictions for $\gamma\gamma \to \mu^+\mu^-$(LPAIR) and for the three lowest Υ states (DIFFVM, normalized to the observed number of events). The arrows indicate the chosen signal region. b) The cross section for elastic photoproduction of $\Upsilon(1S)$ from this analysis with the ZEUS result (which also assumes a 70% contribution of the $1S$ state). The inner and outer error bars show the statistical and the total errors, respectively. Predictions based on pQCD, calculated with the gluon distribution MRSR2 [29], are shown. MRT(1) [15] and FMS [14] are calculations based on the leading order vector meson cross section, including corrections. MRT(2) [15] employs parton hadron duality to derive the prediction for the Υ from the $b\bar{b}$ cross sections.*

In the same $W_{\gamma p}$ range, $d\sigma/dt$ is measured as a function of $W_{\gamma p}$ and t. From this analysis, the parameters of the effective trajectory for elastic J/ψ photoproduction are determined using data from this experiment only. The values of the intercept and the slope of the measured trajectory lie between those of the well known soft and the conjectured hard pomeron trajectories of Donnachie and Landshoff. The measured intercept is compatible with a prediction derived from a NLO BFKL calculation.

Elastic photoproduction of Υ mesons is observed. The cross section for the sum of the three lowest states is measured. The elastic photoproduction cross section for $\Upsilon(1S)$ mesons is extracted. Recent calculations within pQCD are in agreement with this value.

Acknowledgements

We are grateful to the HERA machine group, whose outstanding efforts made this experiment possible. We appreciate the immense effort of the engineers and the technicians who constructed and maintained the detector. We thank the funding agencies for their financial support of the experiment. We wish to thank the DESY directorate for the support and hospitality extended to the non-DESY members of the collaboration. We also thank M. McDermott and T. Teubner for useful discussions and for providing us with their model predictions, W. Koepf for making his program available and H. Spiesberger for discussions on radiative corrections.

$W_{\gamma p}$ interval [GeV]	$\langle W_{\gamma p} \rangle$ [GeV]	$\sigma(\gamma p \to J/\psi p)$ [nb]
26 – 36	31.0	19.8 $\pm$ 3.7 $\pm$ 5.1
40 – 52	46.2	29.8 $\pm$ 3.7 $\pm$ 3.4
52 – 60	56.1	41.7 $\pm$ 5.2 $\pm$ 4.8
60 – 67.8	64.0	49.5 $\pm$ 6.6 $\pm$ 5.6
67.8 – 77	72.5	51.8 $\pm$ 6.9 $\pm$ 5.9
77 – 86	81.5	62.4 $\pm$ 8.5 $\pm$ 7.1
86 – 97	92.0	67.6 $\pm$ 8.8 $\pm$ 7.7
97 – 113	105.2	64.6 $\pm$ 9.6 $\pm$ 7.4
113 – 150	133.4	89.0 $\pm$ 13.2 $\pm$ 12.7
135 – 160	147.3	80.6 $\pm$ 7.9 $\pm$ 12.7
160 – 185	172.2	104.0 $\pm$ 7.9 $\pm$ 16.4
185 – 210	197.1	113.6 $\pm$ 12.2 $\pm$ 18.0
210 – 235	222.4	116.0 $\pm$ 14.8 $\pm$ 18.5
235 – 260	247.4	118.9 $\pm$ 15.6 $\pm$ 19.0
260 – 285	272.4	156.9 $\pm$ 20.3 $\pm$ 25.0

Table 2: *Cross sections for the elastic process $\gamma p \to J/\psi\, p$ in bins of $W_{\gamma p}$. The first error of the cross section is the statistical error and the second is the systematic uncertainty.*

	$W_{\gamma p}$ interval [GeV]					
$-t$ [GeV^2]	$40-54$	$54-66$	$66-78$	$78-91$	$91-110$	$110-150$
$0-0.053$	146.7	231.6	392.4	220.1	348.2	553.5
(0.03)	$\pm$32.5	$\pm$48.4	$\pm$89.3	$\pm$58.7	$\pm$90.1	$\pm$138.7
	$\pm$13.4	$\pm$21.1	$\pm$35.7	$\pm$20.0	$\pm$31.7	$\pm$58.1
$0.053-0.134$	103.8	102.6	140.7	224.9	202.6	219.4
(0.09)	$\pm$21.3	$\pm$20.3	$\pm$80.9	$\pm$45.2	$\pm$43.3	$\pm$64.9
	$\pm$9.4	$\pm$9.3	$\pm$12.8	$\pm$20.5	$\pm$18.4	$\pm$23.0
$0.134-0.25$	48.9	62.0	80.9	125.2	93.4	147.6
(0.19)	$\pm$10.9	$\pm$13.6	$\pm$18.6	$\pm$25.0	$\pm$23.3	$\pm$38.9
	$\pm$4.4	$\pm$5.6	$\pm$7.4	$\pm$11.4	$\pm$8.5	$\pm$15.5
$0.25-0.44$	41.3	40.0	29.5	57.2	64.6	94.6
(0.34)	$\pm$8.8	$\pm$9.4	$\pm$7.5	$\pm$12.6	$\pm$16.0	$\pm$23.1
	$\pm$3.8	$\pm$3.6	$\pm$2.7	$\pm$5.2	$\pm$5.9	$\pm$9.9
$0.44-1.2$	4.82	3.82	5.42	9.62	5.72	11.43
(0.72)	$\pm$1.09	$\pm$0.99	$\pm$1.33	$\pm$2.54	$\pm$1.81	$\pm$3.35
	$\pm$0.44	$\pm$0.35	$\pm$0.49	$\pm$0.88	$\pm$0.52	$\pm$1.20

Table 3: *Differential cross sections $d\sigma/dt$ [nb/GeV^2] for the elastic process $\gamma p \to J/\psi\, p$ in bins of t and $W_{\gamma p}$. The t intervals and bin centres are given in the left column. The first error is statistical and the second is the systematic uncertainty neglecting pure normalization errors.*

References

[1] H1 Coll., S. Aid et al., Nucl. Phys. **B472** (1996) 3.

[2] ZEUS Coll., J. Breitweg et al., Z. Phys. **C75** (1997) 215.

[3] H1 Coll., C. Adloff et al., Eur. Phys. J. **C10** (1999) 373.

[4] ZEUS Coll., J. Breitweg et al., Eur. Phys. J. **C6** (1999) 603.

[5] H1 Coll., S. Aid et al., Nucl. Phys. **B463** (1996) 3;
ZEUS Coll., M.Derrick et al., Z. Phys. **C69** (1995) 39.

[6] M.G. Ryskin, Z. Phys. **C57** (1993) 89;
M.G. Ryskin et al., Z. Phys. **C76** (1997) 231.

[7] L. Frankfurt, W. Koepf and M. Strikman, Phys. Rev. **D54** (1996) 3194.

[8] L. Frankfurt, W. Koepf and M. Strikman, Phys. Rev. **D57** (1998) 512.

[9] P. D. B. Collins, *An Introduction to Regge Theory and High Energy Physics*, Cambridge University Press, Cambridge (1977).

[10] A. Donnachie, P. V. Landshoff, Phys. Lett. **B348** (1995) 213.

[11] for example: A. Capella et al., Phys. Lett. **B337** (1994) 358; M. Bertini et al., Phys. Lett. **B349** (1995) 561; E. Gotsman et al., Phys. Rev. **D49** (1994) 4321.

[12] A. Donnachie, P. V. Landshoff, Phys. Lett. **B437** (1998) 408.

[13] S.J. Brodsky et al., JETP Lett. **70** (1999) 155.

[14] L. Frankfurt, M. McDermott and M. Strikman, JHEP **02** (1999) 002.

[15] A.D. Martin, M.G. Ryskin and T. Teubner, Phys. Lett. **B454** (1999) 339.

[16] H1 Coll., I. Abt et al., Nucl. Instrum. Meth. **A386** (1997) 310 and 348.

[17] H1 Spacal Group, R.-D. Appuhn et al., Nucl. Instrum. Meth. **A386** (1997) 397, ibid. T. Nicholls et al. **A374** (1996) 149.

[18] W. Eick et al., Nucl. Instrum. Meth. **A386** (1997) 81.

[19] P. Merkel, PhD Thesis, Univ. Hamburg (1999), DESY Thesis **99-010**.

[20] J.K. Köhne et al., Nucl. Instrum. Meth. **A389** (1997) 128.

[21] S.P. Baranov et al. in: Proc. of the Workshop on Physics at HERA, ed. W. Buchmüller and G. Ingelman, Hamburg (1992), Vol.3, p. 1478

[22] T. Carli et al. in: Proc. of the Workshop on Physics at HERA, ed. W. Buchmüller and G. Ingelman, Hamburg (1992), Vol.3, p. 1468

[23] B. List, Diploma Thesis, Techn. Univ. Berlin, unpublished (1993);
B. List, A. Mastroberardino in: Proc. of the Workshop on Monte Carlo Generators for HERA Physics, DESY-PROC-1999-02 (1999) 396.

[24] H1 Coll., C. Adloff et al., Phys. Lett. **B421** (1998) 385.

[25] Particle Data Group, C. Caso et al., Eur. Phys. J. **C3** (1998) 1.

[26] E. Fermi, Z. Phys. **29** (1924) 315; C.F. von Weizsäcker, Z. Phys. **88** (1934) 612; E.J. Williams, Phys. Rev. **45** (1934) 729; V.M. Budnev, I.F. Ginzburg, G.V. Meledin, V.G. Serbo, Phys. Rep. **15** (1975) 181.

[27] I. Akushevich in: Proc. of the Workshop on Monte Carlo Generators for HERA Physics, DESY-PROC-1999-02 (1999) 547.

[28] H.L. Lai et al., Phys. Rev. **D55** (1997) 1280.

[29] A.D. Martin, R.G. Roberts and W.J. Stirling, Phys. Lett. **B387** (1996) 419.

[30] M. Glück, E. Reya and A. Vogt, Z. Phys. **C67** (1995) 433.

[31] B.H. Denby et al., E516 Coll., Phys. Rev. Lett. **52** (1984) 795;
M. Binkley et al., E401 Coll., Phys. Rev. Lett. **48** (1982) 73.

[32] ZEUS Coll., G. Abbiendi et al., DESY Report **99-160**.

[33] A. Levy, Phys. Lett. **B424** (1998) 191.

[34] ZEUS Coll., J. Breitweg et al., Phys. Lett. **B437** (1998) 432.